IEEE Photonics Journal
An IEEE Photonics Society Publication

High-Performance Zn-Diffusion 850-nm Vertical-Cavity Surface-Emitting Lasers With Strained InAlGaAs Multiple Quantum Wells

Volume 2, Number 6, December 2010

J.-W. Shi
W.-C. Weng
F.-M. Kuo
Ying-Jay Yang
S. Pinches
M. Geen
A. Joel

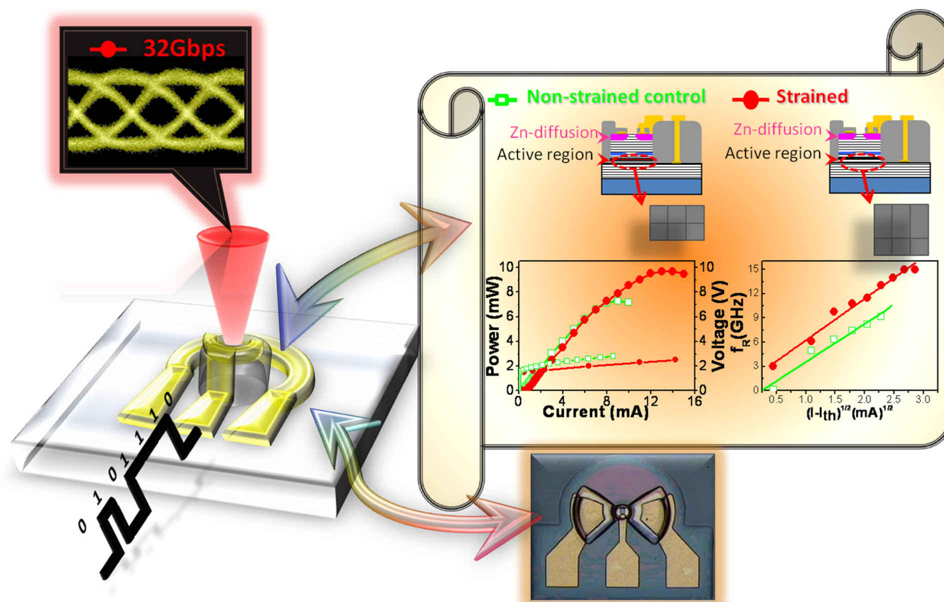

DOI: 10.1109/JPHOT.2010.2089441
1943-0655/$26.00 ©2010 IEEE

IEEE photonics SOCIETY
IEEE

High-Performance Zn-Diffusion 850-nm Vertical-Cavity Surface-Emitting Lasers With Strained InAlGaAs Multiple Quantum Wells

J.-W. Shi,[1] W.-C. Weng,[1] F.-M. Kuo,[1] Ying-Jay Yang,[2] S. Pinches,[3] M. Geen,[3] and A. Joel[3]

[1]Department of Electrical Engineering, National Central University, Taoyuan 320, Taiwan
[2]Department of Electrical Engineering, National Taiwan University, Taipei 106, Taiwan
[3]IQE (Europe) Ltd., Cardiff, CF3 OLW, U.K.

DOI: 10.1109/JPHOT.2010.2089441
1943-0655/$26.00 ©2010 IEEE

Manuscript received September 30, 2010; revised October 13, 2010; accepted October 13, 2010. Date of publication October 21, 2010; date of current version November 9, 2010. This work was supported by the Ministry of Economic Affairs of Taiwan under Grant 98-EC-17-A-07-S1-001. Corresponding author: J.-W. Shi (e-mail: jwshi@ee.ncu.edu.tw).

Abstract: We demonstrate a high-performance Zn-diffusion 850-nm vertical-cavity surface-emitting laser (VCSEL). By the use of strained InAlGaAs/AlGaAs multiple quantum wells for the active region, our structure can have a much higher maximum output power, higher differential quantum efficiency (DQE), and larger modulation current efficiency (D-factor) than those of non-strained control GaAs/AlGaAs VCSELs. Two different Zn-diffusion depths were adopted in our devices with the same single-oxide current-confined aperture ($\sim 6\ \mu m$) to further optimize the static and dynamic performance, respectively. The device with a deep Zn-diffusion depth ($\sim 1.2\ \mu m$) shows an optimized static performance, which includes a low threshold current (0.8 mA), high DQE (90% at ~1.2 mA), and a maximum output power as high as 9.7 mW. On the other hand, the device with a shallow Zn-diffusion depth ($< 0.6\ \mu m$) demonstrates good dynamic performance and exhibits a large D-factor (9.5 GHz/mA$^{1/2}$), high maximum data rate (32 Gbit/s error-free) performance, and very-high data-rate/power-dissipation ratio (5.25 Gbit/s/mW) under an extremely small driving voltage (V_{pp}: 0.25 V).

Index Terms: Semiconductor laser, vertical-cavity surface-emitting laser (VCSEL).

1. Introduction

High-speed, high-efficiency, and low threshold-current (< 1 mA) vertical-cavity surface-emitting lasers (VCSELs) that operate at a wavelength of 850 nm or around 1000 nm have recently attracted a lot of attention due to their suitability for applications in optical interconnects [1]–[9]. There are two important parameters necessary for evaluating power consumption during high-speed VCSEL operation. One is the modulation current efficiency (D-factor), and the other is the threshold current (Ith) [9]. A larger D-factor with a small I_{th} mean makes it possible to achieve a higher modulation speed with less bias current, which means less electrical power dissipation in high-speed VCSEL operation. In order to further improve their performance, GaAs based VCSELs with compressive strained multiple quantum wells (MQWs) (InGaAs/GaAs(P)) at around the 1-μm wavelength regime have been demonstrated with excellent performance [3], [4], [6]–[8]. However, this wavelength regime is not compatible with the traditional 850-nm wavelength used for multi-mode fiber communication. In addition, at this wavelength, only InP-based photoreceiver circuits can be

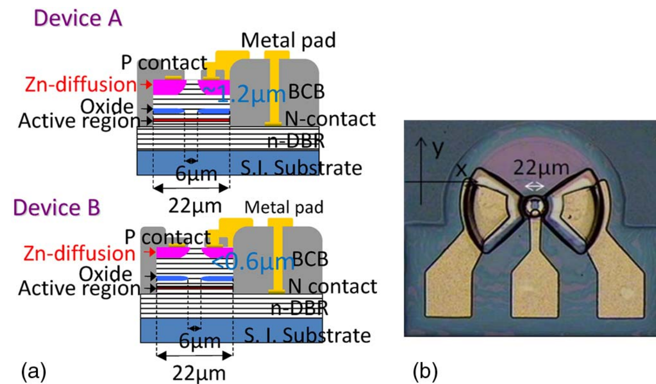

Fig. 1. (a) Cross-sectional views of device A and B and (b) top-view of these two devices. The x- and y-axes, which are specified in our far-field measurement, are defined in (b).

adopted [10], which makes for a higher cost than that of GaAs based photoreceiver circuits at the 850-nm wavelength. The compressively strained Al-free InGaAsP MQWs grown on GaAs substrate is one possible way to realize the edge-emitting lasers [11]–[13] and VCSELs [14] at around 850-nm wavelengths with improved performances compared with those of non-strained GaAs/AlGaAs lasers. In addition, by properly controlling the indium mole fraction and well thickness, compressively strained InGaAs/AlGaAs-based 850-nm VCSELs have also been demonstrated [1], [2], [5]. Although such a device attains a larger D-factor than that of a standard (GaAs/AlGaAs) 850-nm VCSEL, its uniformity of lasing wavelength across the whole epi-wafer is still an issue due to the relative thinner well-width (< 40 Å) required to sustain the 850-nm wavelength [1]. In addition to changing the MQW material, another attractive way to further improve the dynamic performance of VCSELs is to manipulate the number of optical modes inside the VCSEL cavity by the use of the Zn-diffusion technique [9], [15]. In this study, we demonstrated high-performance Zn-diffusion 850-nm VCSELs with InAlGaAs/AlGaAs strained MQWs [16], [17]. Compared with InGaAs/AlGaAs MQWs, we can have a wider well-width and sustain the 850-nm wavelength due to the incorporation of Al. The device with a deep Zn-diffusion depth ($\sim$1.2 μm) and optimized static performance shows a low threshold current (0.8 mA) and a high differential quantum efficiency (DQE) ($\sim$90% at around 1.2 mA) and can have a maximum output power as high as 9.7 mW. On the other hand, devices with a shallow Zn-diffusion depth ($<$ 0.6 μm) can be used for good dynamic performance and exhibit a large D-factor (9.5 GHz/mA$^{1/2}$), high-data rate (32 Gbit/s) and very-high data-rate/power-dissipation ratio (5.25 Gbit/s/mW). Overall, the achieved dynamic and static measurement results are comparable to [1], [2], [5] or even better [14], [17] than those of reported 850-nm VCSELs with compressively strained MQWs.

2. Device Structure and Fabrication

Fig. 1(a) and (b) shows the conceptual cross-sectional and top views of the demonstrated device. Devices A and B with the same diameter of active mesa ($\sim$22 μm) and two different Zn-diffusion depths ($\sim$1.2 and $\sim$0.6 μm) are adopted for optimized static and dynamic performance, respectively [9]. The thick diffusion depth ($\sim$1.2 μm) in device A is used to reduce the p-type contact resistance, significantly minimize the spreading of photon among different optical modes, offer (near) single-mode operation, and improve the static performance of the VCSEL [15]. According to our measurement results, a thicker Zn-diffusion depth ($>$ 1.2 μm) may not further improve the static performance because the lateral Zn-diffusion width significantly shades our optical aperture (with a 6-μm width in original), which results in the tremendous increase of internal loss inside the optical cavity. In addition, the significant spatial hole-burning effect in these (near) single-mode VCSELs with a thick diffusion depth ($>$ 0.6 μm) will cause significant low-frequency rolloff, which seriously degrades the quality of eye-pattern of VCSELs [9], [15], [18].

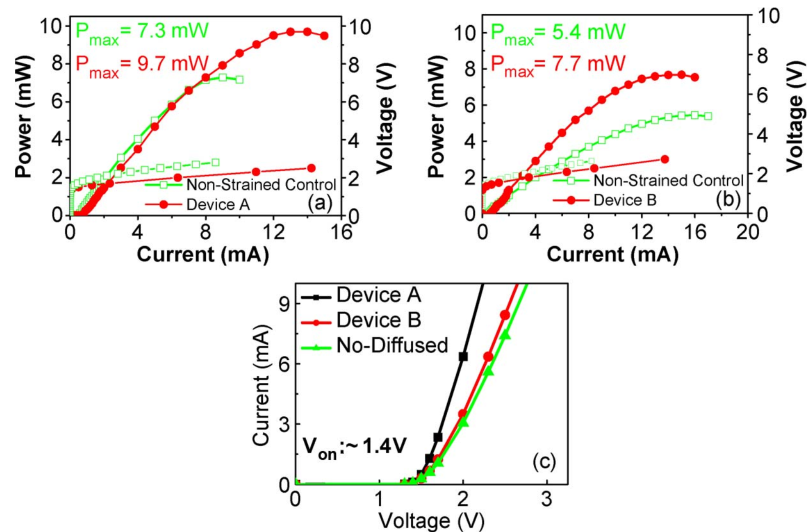

Fig. 2. Characteristics of the optical output power (L) and voltage (V) versus biasing current (I) for devices A (a) and B (b) compared with the controls with the same Zn-diffusion depths but with non-strained MQWs. (c) Measured *I–V* curves of devices A and B and the non-diffused control.

Although the shallow Zn-diffusion depth in device B cannot ensure pure single-mode operation, compared with that of the non-diffusion VCSEL, it can still minimize the spreading of photons among multiple mutually incoherent modes and enhance the value of the D-factor [9]. An epi-layer structure was grown on a semi-insulating GaAs substrate, which is composed of three $In_{0.15}Al_{0.1}Ga_{0.75}As/Al_{0.3}Ga_{0.7}As$ MQWs sandwiched between a 30-pair n-type and a 20-pair p-type $Al_{0.9}Ga_{0.1}As/Al_{0.12}Ga_{0.88}As$ Distributed-Bragg-Reflector (DBR) layer with an $Al_{0.98}Ga_{0.02}As$ layer above the MQWs for oxidation. Compared with that reported for $In_{0.1}Ga_{0.9}As/Al_{0.37}Ga_{0.63}As$ strained 850-nm VCSELs [1], we can achieve a higher indium mole fraction (0.15 versus 0.1) with a thicker well-width (50 versus 40 Å). This is due to the incorporation of Al, which enlarges the bandgap but has no significant influence on the lattice constant (strain) of the well layer [16]. Our strained VCSEL has a higher indium mole fraction and wider well-width than those of InGaAs based strained 850-nm VCSELs [1], [2] which lead to a more significant improvement in static/dynamic performance and uniformity of the wafer, respectively. An oxidation technique is used to define a circular current-confined area that is 6 μm in diameter. The multiple oxide layers are usually adopted in the very-high speed (> 30 Gbit/sec) 850-nm VCSEL to further reduce its high parasitic capacitance [1], [2], [5], [6]. However, the stress of these multiple oxide layers on the active regions may degrade the reliability and current-voltage (*I–V*) performance of the VCSEL [2], [19], which should limit its high-speed performance under high ambient temperature ($\sim$85 $^\circ$C) operation. Here, we simply adopt the single-oxide layer in our structure. The diameter of the optical aperture (without Zn-diffusion) is around 5 μm, as shown in Fig. 1(a); details of the fabrication process have been given in our previous work [9].

3. Measurement Results

Fig. 2(a) and (b) shows a comparison of the light output and bias voltage versus current (*L–I* and *V–I*) of devices A and B with that of the control 850-nm VCSELs, which have GaAs/AlGaAs MQW layers (non-strained), the same Zn-diffusion depths, and the same diameter of oxide aperture, respectively. Fig. 2(c) shows the bias current versus voltage (*I–V*) characteristics of devices A and B and the device without Zn-diffusion. As can be seen in Fig. 2(a), the measured *L–I* curve of device A clearly shows a comparable threshold current ($\sim$0.8 mA), a comparable maximum external quantum efficiency ($\sim$90% at around 1.2 mA), and a significantly higher maximum output power (9.7 versus 7.3mW) than those of the non-strained control device. A similar result can also be obtained for the

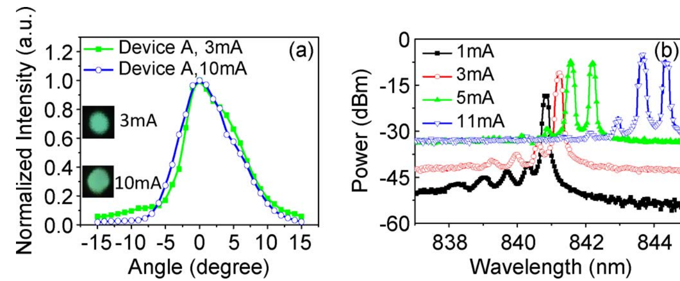

Fig. 3. (a) Measured 1-D far field patterns in the *x*-directions under different current levels. The insets show 2-D images of the far-field patterns under low (near threshold) and high bias currents (near saturation). (b) Measured output optical spectra under different bias currents.

device B, as shown in Fig. 2(b). The superior maximum saturation power performance of device A and B to non-strained controls can be attributed to the improved *I–V* performance of strained devices, as shown in Fig. 2(a) and (b). The required bias voltage of device A and non-strained control under 2 mA bias current is around 1.7 and 2.1 V, respectively. A smaller turn-on voltage of strained devices indicates lower electrical power dissipation and less device heating, and an improved high-power performance of device A and B can thus be expected. In addition, the measured *I–V* curves in Fig. 2(c) indicate that a deeper Zn-diffusion depth in the VCSEL with strained MQWs leads to a lower contact resistance. Device A under a 10-mA bias current has a differential resistance as low as 65 Ω, which is much lower than that typically reported for high-speed VCSELs with the same or even larger diameters of oxide aperture $(\sim 100\ \Omega)$ [1]–[8]. This was possible because of the p-type Ohmic contacts on the Zn-diffused region, which led to disordering of DBR layers and reduced device resistance [9], [15]. The one-dimensional (1-D) far-field patterns of device A were measured under different operating currents using a rotational arm, a mounted slit, and a photodetector. The results are shown in Fig. 3(a). The insets to (a) show 2-D images of the far-field patterns obtained under low bias currents (3 mA, near the threshold) and high bias currents (10 mA, near saturation). We can clearly see that single-spot output can be achieved for the whole range of bias currents. Furthermore, the measured full-width at half-maximum (FWHM) of the 1-D far field pattern is around 9°, which is close to the calculated ideal diffraction-limited divergence angle (around 8°) of a Zn-diffusion aperture with a diameter of around 5 μm. This result indicates the (near) single-mode performance of device A. Fig. 3(b) shows the output optical spectra of device A. We can clearly see that when the bias current reaches 5 mA, the multi-mode phenomenon starts to happen in our device. The high-speed electrical-to-optical (E-O) performance of fabricated device A and B were measured by a lightwave component analyzer (LCA), which was composed of a network analyzer (Anritsu 37397C) and a calibrated 25 GHz photoreceiver module (New focus 1481-S). Fig. 4(a) and (b) shows the measured E-O response under different bias currents at room temperature (RT) of device A and B, respectively. Fig. 4(c) shows the extracted relaxation oscillation frequency (f_R) [based on the shown E-O response in (a)] versus $\sqrt{I - I_{th}}$ of device B and non-strained control with the same Zn-diffusion depth, where I is the bias current, and I_{th} is the threshold current. The slope (D) of these fitting lines can be used to evaluate how fast the f_R increases with the bias current [9], [15], which is a key factor for optical interconnects, as discussed before. Although device A can achieve excellent DC performance with a near single-mode output, it still suffers serious low-frequency rolloff at around 3 GHz, as shown in Fig. 4(a), which become more serious under high bias current. Such a phenomenon has been reported for those of the single-mode VCSEL [9], [15], [18] and can be attributed to the reported spatial–hole-burning effect [9], [15], [18], which means that the single-mode Gaussian distribution of the output far-field of device A results in a photon concentration at the center of aperture, which has a short carrier simulated recombination time (hundreds of picoseconds). However, in the periphery of the aperture, where the photon density is relative low, the carrier recombination time is longer than in the center [18]. Under high-frequency AC signal modulation, the change of peripheral carriers cannot keep up with the speed of the swing in the AC voltage, which thus results in the observed low-frequency roll-off phenomenon. It is thus preferred that device B have a shallow Zn-diffusion depth

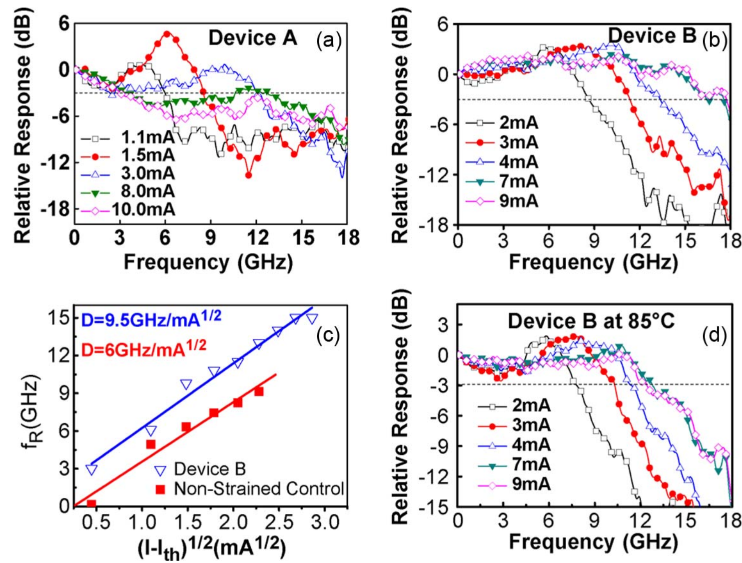

Fig. 4. (a) E-O frequency responses of device A measured under different bias currents at RT. (b) E-O frequency responses of device B measured under different bias currents at RT. (c) Measured f_R versus $(I - I_{th})^{1/2}$ and the extracted D factors of device B and control with non-strained MQWs at RT. (d) E-O frequency responses of device B measured under different bias currents at 85 °C.

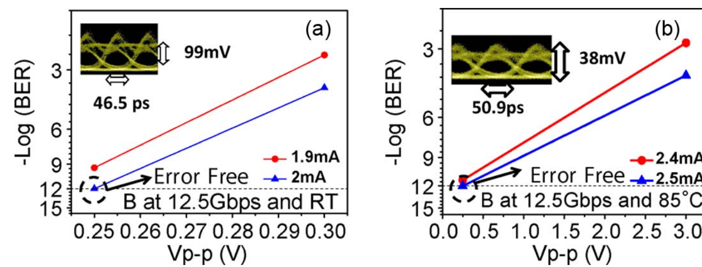

Fig. 5. BER versus V_{pp} measured under different bias currents for device B at (a) 12.5 Gbit/s, RT operation and (b) 12.5 Gbit/s and 85 °C operation. The insets show the corresponding eye-pattern under lowest bias current and V_{pp} operation.

with a multi-mode output and a more uniform optical far-field distribution to minimize the spatial hole-burning effect and achieve optimized dynamic performance [9]. It can be seen by looking at Fig. 4(b) and (c) that, due to the low threshold-current and high DQE performance discussed above, the extracted D factor of device B can be as high as (9.5 GHz/mA$^{1/2}$). Such a value is much larger than that of non-strained control and reported InGaAs/AlGaAs 850-nm VCSEL (9.5 GHz/mA$^{1/2}$ versus 7.7 GHz/mA$^{1/2}$ [1]). Overall, these static/dynamic measurement results indicate that our strained InAlGaAs/AlGaAs MQWs not only have improved DC but also improve dynamic performance of the VCSEL. High-speed operation under ambient temperature as high as 85 °C of the VCSEL is also a key issue for practical application. Fig. 4(d) shows the measured E-O responses of device B under different bias currents at 85 °C. Compared with the RT measurement results, as shown in Fig. 4(b), we can clearly see that when the bias current reaches 3 mA, significant degradation of speed can be observed (18 to 13 GHz at 7 mA). On the other hand, under a low bias current ($<$ 3 mA), such a phenomenon is not significant. This result implies that the device-heating effect under high bias current and high-temperature operation seriously limits the maximum modulation speed of the VCSEL. Fig. 5(a) and (b) shows the measured $-$log(bit error rate) (BER) versus V_{pp} of device B under different bias currents at RT and 85 °C operation, respectively. The length of the used 12.5-Gbit/s pseudo random binary sequence (PRBS) pattern is $2^{15} - 1$. The same photoreceiver module is used as in the LCA

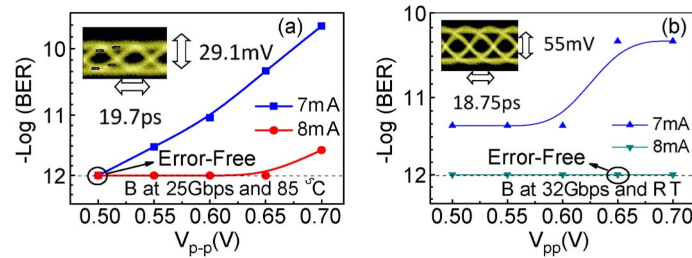

Fig. 6. BER versus V_{pp} measured under different bias currents for device B at (a) 25 Gbit/s, 85 °C operation, and (b) 32 Gbit/s and RT operation. The insets show the corresponding eye pattern under lowest bias current and V_{pp} operation.

measurements, but an additional broadband (near DC to 65 GHz) amplifier (Centellax UA0L65VM) is used for eye-pattern measurement. The insets show the corresponding eye-patterns for the lowest bias current and V_{pp} operations. As can be seen, even under such extremely low bias current (2 mA) and RF driving voltage ($0.25V_{pp}$), 12.5-Gbit/s error-free ($BER < 10^{-12}$) operation can be achieved. The corresponding data-rate/power-dissipation ratio can be as high as 5.25 Gbit/s/mW, which is superior to that of a high-performance ~1000-nm VCSEL for error-free data transmission at 10 Gbit/s [8] and 35 Gbit/s [6] (5.25 versus 3.5 Gbit/s/mW [6]). The dissipated power of our device is defined as the difference between the output optical output power and the injected electrical power [6]. On the other hand, as shown in Fig. 5(b), when the ambient temperature reaches 85 °C, the required bias current for error-free operation slightly increases to 2.5 mA. As discussed in Fig. 4(d), under such low bias current (< 3 mA), the degradation in speed under high-temperature operation is not a serious issue. The 0.5-mA penalty of the required bias current for 12.5-Gbit/s error-free operation at 85 °C can be attributed to the degradation in DQE of the VCSEL, which results in a smaller eye height than that operated under RT, as shown in the insets of Fig. 5. Fig. 6(a) and (b) shows the measured $-\log(BER)$ versus V_{pp} at further higher data rates of 25 and 32 Gbit/s for back-to-back transmission, respectively. The measured temperature for 25- and 32-Gbit/s operation is 85 °C and RT, respectively. The insets show the corresponding eye-patterns for the lowest bias current and V_{pp} operations. As can be seen, even under 85 °C, 25-Gbit/s error-free operation can be achieved under 7-mA bias current and a V_{pp} as small as 0.5 V. Under such a low bias current, the measured BER is raised with the increase of V_{pp}. On the other hand, when the bias current reaches 8 mA, this phenomenon disappears, and the measured BER is insensitive to the value of V_{pp}. Such a result can be attributed to the fact that under a 7-mA bias current, the speed of the VCSEL is marginal for 25-Gbit/s eye-opening, and a large V_{pp} swing may seriously distort the eye pattern and degrades the BER performance. Similar dynamic behaviors have also been observed at 12.5-Gbit/s low-bias current (2 mA) operation, as shown in Fig. 5(a) and (b). Furthermore, as shown in Fig. 6(b), under RT operation, the highest error-free data rate can be as high as 32-Gbit/s under an 8-mA bias current. However, under 85 °C operation, our VCSEL cannot sustain such a high bit-rate operation due to degradation of its 3-dB E-O bandwidth with the increase of ambient temperature under high bias current (> 3 mA), as discussed in Fig. 4(d).

4. Conclusion

We demonstrated the high-performance Zn-diffusion 850-nm VCSELs with strained InAlGaAs/AlGaAs MQWs. Devices with a deep Zn-diffusion depth (~1.2 μm) show excellent DC performance, which includes low differential resistance (~65 Ω), low threshold current (~0.8 mA), high DQE (~90%), and high maximum output power (9.7 mW). On the other hand, devices with a shallow Zn-diffusion depth exhibit a large D-factor (9.5 GHz/mA$^{1/2}$), high maximum operation speed (32 Gbit/s), and a data-rate/power-dissipation ratio as high as 5.25 Gbit/s/mW. These results clearly indicate that the strained InAlGaAs/AlGaAs MQWs and Zn-diffusion technique can effectively improve both DC and dynamic performance of 850-nm VCSELs.

References

[1] S. B. Healy, E. P. O'Reilly, J. S. Gustavsson, P. Westbergh, A. Haglund, A. Larsson, and A. Joel, "Active region design for high-speed 850-nm VCSELs," *IEEE J. Quantum Electron.*, vol. 46, no. 4, pp. 506–512, Apr. 2010.

[2] P. Westbergh, J. S. Gustavsson, B. Kogel, A. Haglund, A. Larsson, A. Mutig, A. Nadtochiy, D. Bimberg, and A. Joel, "40 Gb/sec error-free operation of oxide-confined VCSEL," *Electron. Lett.*, vol. 46, no. 14, pp. 1014–1016, Jul. 2010.

[3] H. Hatakeyama, T. Anan, T. Akagawa, K. Fukatsu, N. Suzuki, K. Tokutome, and M. Tsuji, "Highly reliable high-speed 1.1-μm-range VCSELs with InGaAs/GaAsP-MQWs," *IEEE J. Quantum Electron.*, vol. 46, no. 6, pp. 890–897, Jun. 2010.

[4] K. Yashiki, N. Suzuki, K. Fukatsu, T. Anan, H. Hatakeyama, and M. Tsuji, "1.1-μm-range high-speed tunnel junction vertical-cavity surface-emitting lasers," *IEEE Photon. Technol. Lett.*, vol. 19, no. 23, pp. 1883–1885, Dec. 2007.

[5] S. A. Blokhin, J. A. Lott, A. Mutig, G. Fiol, N. N. Ledentsov, M. V. Maximov, A. M. Nadtochiy, V. A. Shchukin, and D. Bimberg, "Oxide-confined 850 nm VCSELs operating at bit rates up to 40 Gb/s," *Electron. Lett.*, vol. 45, no. 10, pp. 501–503, May 2009.

[6] Y.-C. Chang, C. S. Wang, and L. A. Coldren, "High-efficiency, high-speed VCSELs with 35 Gb/s error-free operation," *Electron. Lett.*, vol. 43, no. 19, pp. 1022–1023, Sep. 2007.

[7] C.-K. Lin, A. Tandon, K. Djordjev, S. W. Corzine, and M. R. T. Tan, "High-speed 985 nm bottom-emitting VCSEL arrays for chip-to-chip parallel optical interconnects," *IEEE J. Sel. Topics Quantum Electron.*, vol. 13, no. 5, pp. 1332–1339, Sep./Oct. 2007.

[8] J. B. Heroux, M. Tokunari, K. Takaki, and S. Nakagawa, "Low power optical interconnect at 10 Gbit/s with high efficiency 1060 nm VCSEL," in *Proc. CLEO/QELS*, San Jose, CA, 2010, pp. 1–2.

[9] J.-W. Shi, C.-C. Chen, Y.-S. Wu, S.-H. Guol, and Y.-J. Yang, "The influence of Zn-diffusion depth on the static and dynamic behaviors of Zn-diffusion high-speed vertical-cavity surface-emitting lasers at a 850 nm wavelength," *IEEE J. Quantum Electron.*, vol. 45, no. 7, pp. 800–806, Jul. 2009.

[10] K. Fukatsu, K. Shiba, Y. Suzuki, N. Suzuki, T. Anan, H. Hatakeyama, K. Yashiki, and M. Tsuji, "30 Gb/s over 100-m MMFs using 1.1-μm range VCSELs and photodiodes," *IEEE Photon. Technol. Lett.*, vol. 20, no. 11, pp. 909–911, Jun. 2008.

[11] T. E. Sale, C. Amamo, Y. Ohiso, and T. Kurokawa, "Using strained $(Al_xGa_{1-x})_yIn_{1-y}As_zP_{1-z}$ system materials to improve the performance of 850 nm surface- and edge-emitting lasers," *Appl. Phys. Lett.*, vol. 71, no. 8, pp. 1002–1004, Aug. 1997.

[12] A. Al-Muhanna, J. K. Wade, T. Earles, J. Lopez, and L. J. Mawst, "High-performance, reliable, 730-nm-emitting Al-free active region diode lasers," *Appl. Phys. Lett.*, vol. 73, no. 20, pp. 2869–2871, Nov. 1998.

[13] N. Tansu, D. Zhou, and L. J. Mawst, "Low-temperature sensitive, compressively strained InGaAsP active ($\lambda = 0.78 - 0.85$ μm) region diode lasers," *IEEE Photon. Technol. Lett.*, vol. 12, no. 6, pp. 603–605, Jun. 2000.

[14] N. Tansu and L. J. Mawst, "Compressively-strained InGaAsP-active ($\lambda = 0.85$ μm) VCSELs," in *Proc. IEEE LEOS*, Rio Grande, Puerto Rico, Nov. 2000, vol. 2, pp. 724–725.

[15] J.-W. Shi, C.-C. Chen, Y.-S. Wu, S.-H. Guol, and Y.-J. Yang, "High-power and high-speed Zn-diffusion single fundamental-mode vertical-cavity surface-emitting lasers at 850 nm wavelength," *IEEE Photon. Technol. Lett.*, vol. 20, no. 13, pp. 1121–1123, Jul. 2008.

[16] C. A. Wang, J. N. Walpole, L. J. Missaggia, J. P. Donnelly, and H. K. Choi, "AlInGaAs/AlGaAs separated-confinement heterostructure strained single quantum well diode lasers grown by organometallic vapor phase epitaxy," *Appl. Phys. Lett.*, vol. 58, no. 20, pp. 2208–2210, May 1991.

[17] J. Ko, E. R. Hegblom, Y. Akulova, N. M. Margalit, and L. A. Coldren, "AlInGaAs/AlGaAs strained-layer 850 nm vertical-cavity lasers with very low thresholds," *Electron. Lett.*, vol. 33, no. 18, pp. 1550–1551, Aug. 1997.

[18] J. S. Gustavsson, Å. Haglund, J. Bengtsson, P. Modh, and A. Larsson, "Dynamic behavior of fundamental-mode stabilized VCSELs using shallow surface relief," *IEEE J. Quantum Electron.*, vol. 40, no. 6, pp. 607–619, Jun. 2004.

[19] S. Xie, R. Herrick, G. D. Brabander, W. Widjaja, U. Koelle, A.-N. Cheng, L. Giovane, F. Hu, M. Keever, T. Osentowski, S. McHugo, M. Mayonte, S. Kim, D. Chamberlin, S. J. Rosner, and G. Girolami, "Reliability and failure mechanisms of oxide VCSELs in non-hermetic environments," *Proc. SPIE*, vol. 4994, pp. 173–180, 2003.